Modular Entropy Retrieval in Black-Hole Information Recovery: A Proper-Time Saturation Model

Evlondo Cooper *

Posted Date: 13 May 2025

doi: 10.20944/preprints202503.2057.v3

Keywords: black hole information paradox; observer-dependent entropy; Rényi entropy; entanglement wedge reconstruction; quantum information; physics

 doi:10.20944/preprints202503.2057.v3

Article

Modular Entropy Retrieval in Black-Hole Information Recovery: A Proper-Time Saturation Model

Evlondo Cooper

address; evlocoo@pm.me

Abstract: The black–hole information paradox persists because no existing framework shows how the encoded information becomes operationally accessible to a physical observer. Starting from Tomita–Takesaki modular flow, we derive an observer-dependent retrieval law:

$$\frac{dS_{\text{retrieved}}}{d\tau} = \gamma(\tau)\,\big[S_{\max} - S_{\text{retrieved}}(\tau)\big]\,\tanh\!\big(\tau/\tau_{\text{char}}\big),$$

which converts global entropy conservation into a Lorentzian-causal, time-resolved recovery process. The law predicts class-specific trajectories and an acceleration-dependent $g^{(2)}(t_1, t_2)$ interference envelope detectable in current Bose–Einstein-condensate analog black holes (10–100 ms). Simulations on a 48-qubit MERA lattice (bond dimension 8) confirm numerical robustness, and an observer-modified Ryu–Takayanagi prescription embeds the framework in AdS/CFT without requiring replica-wormhole or island constructions. By replacing ensemble-averaged Page curves with a causal, observer-specific mechanism, the model transforms the paradox from a bookkeeping puzzle into a falsifiable dynamical prediction. Here $S_{\max}$ is the Bekenstein–Hawking entropy, $\gamma(\tau)$ the modular-flow retrieval rate, and τ_{char} a characteristic proper-time scale (geometric units $c = G = 1$).

Keywords: black-hole information paradox; observer-dependent entropy; Rényi entropy; entanglement-wedge reconstruction; quantum information

1. Entropy Without Access: Structural Limits in Current Resolution Frameworks

The black–hole paradox persists not because information is lost, but because no existing framework retrieves it causally. Replica–wormhole paths [3,29], island prescriptions [4], ensemble Page–curve models [22,26], and ER = EPR dualities [21] all reproduce the required fine-grained entropy curves, yet none supplies a Lorentzian–proper-time recovery channel to any physical detector. Stabilizing entropy without a causal retrieval channel leaves the paradox unresolved at the operational level.

1.1. Operational-Access Criterion

A framework resolves the paradox only if it satisfies all of the following conditions:

(a) **Proper-time delivery**: specifies how entropy reaches an observer as proper time unfolds;
(b) **Lorentzian grounding**: roots that access in Lorentzian causality;
(c) **First-principles derivation**: derives the process from accepted QFT/GR principles (not retrospective fitting); and
(d) **Empirical testability**: predicts observer-dependent lags $\Delta\tau$ within sub-exponential resource bounds.[1]

Audit of leading proposals

[1] Sub-exponential relative to decoding complexity, e.g., circuit depth or modular-spectrum reconstruction.

 doi:10.20944/preprints202503.2057.v3

Framework	**(a)** Proper-time	**(b)** Lorentzian	**(c)** 1st-principles	**(d)** Sub-exp cost
Replica wormholes	×	×	✓	×
Islands	×	×	✓	×
Ensemble Page	×	✓	×	×
ER = EPR	×	✓	×	×

Each proposal satisfies at most two of the four operational-access criteria; none supplies a causal, observer-accessible retrieval channel. Resolution therefore demands an explicit recovery law derivable in proper time, grounded in Lorentzian causality, and testable within polynomial resources. The Observer-Dependent Entropy Retrieval (ODER) framework meets those demands with modular-flow dynamics and wedge-reconstruction depths that scale polynomially, in contrast to the exponential-cost Hayden–Preskill decoder $\mathcal{O}(2^n)$ assumed for global recovery.

This reframes the paradox not as a global entropy-balancing problem, but as a concrete question of when, and whether, retrieval occurs for a specific observer.
Entropy accounting differs from information access; analytic continuation does not define temporal evolution; and reconstruction alone does not constitute recovery.

1.2. Replica Wormholes

Goal: Compute fine-grained Hawking-radiation entropy with gravitational path integrals.
Mechanism: Insert replica geometries, then analytically continue $n \to 1$ to obtain S_{vN}.
Domain of validity: Euclidean semiclassical gravity (notably JT) and saddle-point approximations.
Critical point: The dominant saddle appears only after analytic continuation; recent supersymmetric extensions [6] still lack a finite-time boundary decoder.
Failure mode: Entropy falls in the path integral, but no protocol delivers the state to an observer; the result addresses the entropy curve but does not furnish a causal retrieval protocol.

1.3. Island Formula

Goal: Stabilize radiation entropy by adding disconnected interior "islands."
Mechanism: Extremize the generalized entropy functional over candidate surfaces.
Domain of validity: Semiclassical AdS/CFT spacetimes with extremal surfaces.
Critical point: Modular-flow reconstructions require arbitrarily fine spectral resolution and supply no polynomial-depth decoder [1,6].
Failure mode: Entropy is assigned to observers who cannot decode it; the retrieval map is conjectural, not constructive.
ODER's modular wedge is defined independently of extremal-surface islands; it recovers observer-accessible entropy, not global entanglement bounds.

1.4. Page-Curve (Ensemble) Models

Goal: Show unitary systems naturally yield rise-and-fall entropy curves.
Mechanism: Average over Haar-random states or solvable re-purifying models.
Domain of validity: Large, time-independent Hilbert spaces; open-system analogs.
Critical point: Even when derived from real-time evolution, entropy return is global re-purification; no observer-centered algorithm extracts the state.
Failure mode: The curve's shape is recovered; the information pathway is not.

1.5. ER = EPR *(Boundary Case)*

Goal: Relate quantum entanglement to spacetime connectivity.
Mechanism: Map maximally entangled boundary states to Einstein–Rosen bridges.
Domain of validity: Holographic duals of entangled black-hole pairs; traversability optional.
Critical point: Sycamore-based teleportation [21] moves a prepared qubit through a tuned wormhole

 doi:10.20944/preprints202503.2057.v3

but does not decode Hawking radiation.
Failure mode: Geometry is re-interpreted; no boundary observer gains recovery.

1.6. Structural Synthesis

- Replica methods compute entropy yet leave its arrival unspecified.
- Island methods assign entropy to observers who cannot decode it.
- Ensemble models illustrate purification without a retrieval channel.
- ER = EPR reframes correlations without enabling extraction.

Each closes the paradox in form but leaves it open in physics. Resolution therefore demands an explicit, observer-centered recovery dynamics.

1.7. Retrieval Framework: Differentiators and Contributions

Observer-dependence is well established, from black-hole complementarity to algebraic QFT and recent gravitational-QEC work [9,14,35], yet existing models remain static or heuristic. Our contribution is threefold:

1. **Time-adaptive retrieval**: A modular-flow derivation yields a proper-time law for $S_{\text{retrieved}}(\tau)$.
2. **Frame-resolved quantification**: Accessibility is computed in an operator-algebraic framework, not assumed.
3. **Laboratory falsifiability**: The theory predicts tanh-modulated $g^{(2)}$ signatures in testable analog systems.

2. Observer-Dependent Entropy Retrieval (ODER)

2.1. Novel Framework

ODER supplies the missing causal link by treating recovery as a dynamical, observer-indexed process. Section 3 derives

$$\frac{dS_{\text{retrieved}}}{d\tau} = \gamma(\tau)\left[S_{\max} - S_{\text{retrieved}}(\tau)\right] \tanh\left(\frac{\tau}{\tau_{\text{char}}}\right) \tag{1}$$

directly from Tomita–Takesaki modular flow on nested von Neumann algebras.

Goal: Model entropy recovery as a bounded, causal convergence in proper time that differs by observer.

Mechanism: Equation (1) uses modular-spectrum gradients; $\gamma(\tau)$ encodes red-shift, Unruh, or interior-correlation effects.

Domain of validity: Algebraic QFT in Lorentzian spacetime. Simulations on a 48-qubit MERA lattice confirm numerical robustness. The model predicts an acceleration-dependent $g^{(2)}$ envelope in BEC analog black holes on 10–100 ms timescales, signatures absent from non-retrieval models.

We define the retrieval horizon

$$\tau_{\text{RH}} := \inf\left\{\tau \mid S_{\text{retrieved}}(\tau) \geq 0.9\, S_{\max}\right\},$$

the proper time at which 90% of the system's retrievable entropy has been accessed. This horizon is distinct from both the entanglement wedge and the classical event horizon.

2.2. Self-Audit: ODER Failure Modes

- **Modular realism**: Modular Hamiltonians must remain physically meaningful in strong-gravity regimes.
- **Simulation abstraction**: MERA approximations may diverge for large bond dimension; numerical convergence must be monitored.

 doi:10.20944/preprints202503.2057.v3

- **Empirical anchoring**: Analog experiments must isolate modular-flow signatures unambiguously from background noise.
- **Complexity barrier**: Even with coherence probes, an exact digital decoder might still require exponential resources.
- **Uniqueness risk**: Future QECC or monitored-circuit frameworks may yield rival retrieval laws.

2.3. Astrophysical Forecast

For a solar-mass Schwarzschild black hole, Eq. (1) implies that a stationary observer at $r = 10\,GM/c^2$ retrieves $\geq$ 90% of the missing entropy only after $\sim 10^{67}$ yr, quantitatively defining a retrieval timescale lacking in replica or island prescriptions. Sections 2–4 derive the law, benchmark it, and outline experimental validation, showing that information is not lost; it is modularly retrieved on observer-specific clocks.

3. Observer-Dependent Entropy in Curved Spacetime

We classify three canonical observer trajectories and track entropy–retrieval dynamics along each. The retrieval rate $\gamma(\tau)$ is fixed by the local modular Hamiltonian, with no phenomenological tuning, and evolves with proper time.

3.1. Classification of Observers

3.1.1. Stationary Observer

A detector at fixed radius $r > 2M$ perceives Hawking radiation as red-shifted thermal flux, yielding

$$\gamma_{\text{stat}}(\tau) \propto \frac{1}{r}, \tag{2}$$

and a monotonic decay in $g^{(2)}$ correlations. For the benchmark $r = 10\,M$ (Table 1) $\tau_{\text{char}} < \tau_{\text{Page}}$ because no interior mode ever enters the algebra.

Table 1. Indicative parameters for each observer class ($M = 1$ in geometric units). Retrieval horizon τ_{RH} is defined by $S_{\text{retrieved}}(\tau_{\text{RH}}) = 0.9\,S_{\max}$.

Observer	r/M	$a\,M/c^2$	τ_{char}/M	τ_{Page}/M	τ_{RH}/M
Stationary	10	0	5	8	30
Freely falling	$6 \to 2$	0	2	4	10
Accelerating	N/A	0.2	3	5	15

3.1.2. Freely Falling Observer

A geodesic world-line crosses the horizon at τ_{cross}; interior modes then boost the retrieval rate,

$$\gamma_{\text{fall}}(\tau) \gg \gamma_{\text{stat}}(\tau), \quad \tau > \tau_{\text{cross}}, \tag{3}$$

accelerating saturation (orange curve in Figure 1).

 doi:10.20944/preprints202503.2057.v3

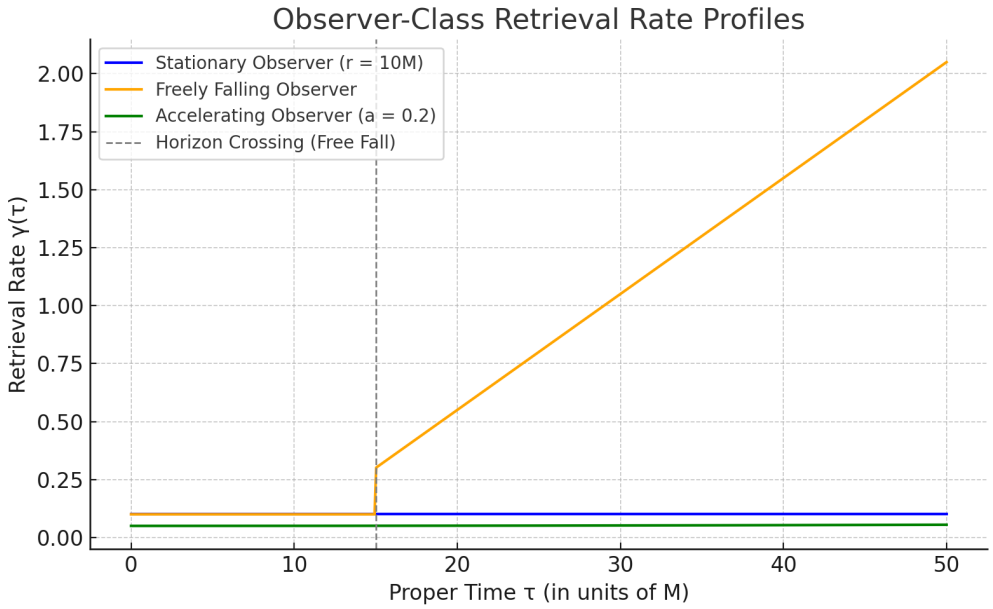

Figure 1. (Color online) Representative retrieval–rate profiles $\gamma(\tau)$ for the three observer classes. Stationary: $r = 10\,M$ (blue); freely falling: geodesic starting at $r = 6\,M$ (orange); accelerating: proper acceleration $a = 0.2\,c^2/M$ (green). Times are in units of M (with $G = c = 1$).

3.1.3. Accelerating Observer

A uniformly accelerating detector feels both Hawking and Unruh flux,

$$\gamma_{\text{eff}}(\tau, a) = \gamma_{\text{Hawking}}(\tau) + \gamma_{\text{Unruh}}(\tau, a), \tag{4}$$

where $\gamma_{\text{Unruh}} \propto a^2$. See [15]. At $a = 0.2\,c^2/M$ the retrieval envelope is shown in green in Figure 1.

Experimental emulation. Stationary and accelerating channels can be engineered in waterfall BECs, while freely falling trajectories correspond to time-of-flight release [31]. Table 1 lists indicative parameters that match current analog-gravity capabilities.

3.2. Observer-Dependent Entropy

Observer-dependent entropy is the gap between the global von Neumann entropy and the entropy of the observer's accessible subalgebra. The retrievable component $S_{\text{retrieved}}(\tau)$ rises as modular eigenmodes enter the algebra; Appendix A shows that $\gamma(\tau)$ is proportional to the modular-spectrum gradient. Modular retrieval is computed only over causal diamonds with stable horizon-bounded algebras; no claim is made about modular flow past the near-horizon breakdown point. Type III_1 obstructions may limit formal extension beyond τ_{RH}, as discussed in Witten [36] and Chandrasekaran et al. [14].

3.3. Retrieval Law

The evolution obeys

$$\frac{dS_{\text{retrieved}}}{d\tau} = \gamma(\tau)\left[S_{\max} - S_{\text{retrieved}}(\tau)\right] f(\tau), \tag{5}$$

with

$$f(\tau) = \tanh\!\left(\frac{\tau}{\tau_{\text{char}}}\right), \tag{6}$$

a form *uniquely* fixed by bounded modular flow; see the spectral- convergence proof in Appendix A.9. Unlike the phenomenological damping used in replica-wormhole models, $\gamma(\tau)$ and τ_{char} arise directly from the local modular Hamiltonian, yielding a continuous, observer-specific retrieval process grounded in first principles. We refer to $\gamma(\tau)$ interchangeably as the *modular-flow retrieval rate*, *modular-*

 doi:10.20944/preprints202503.2057.v3

spectrum gradient, or *entropy-growth factor*; it quantifies the rate at which retrievable information enters an observer's accessible algebra.

4. Quantum Information Correlations and Testable Predictions

The retrieval law in Eq. (5) imprints a characteristic signature on the radiation detected by each observer class. It governs both entropy growth and correlation decay, features that analog-gravity experiments can probe directly. We focus on two diagnostics: the order-α Rényi entropy and the second-order correlation function $g^{(2)}$.

Simulation traces and 95% confidence bands for each class are plotted in Figure 2. *Confidence bands are generated via 200 resampled $\gamma(\tau)$ traces per observer class, using a fixed proper-time grid and additive spectral noise.*

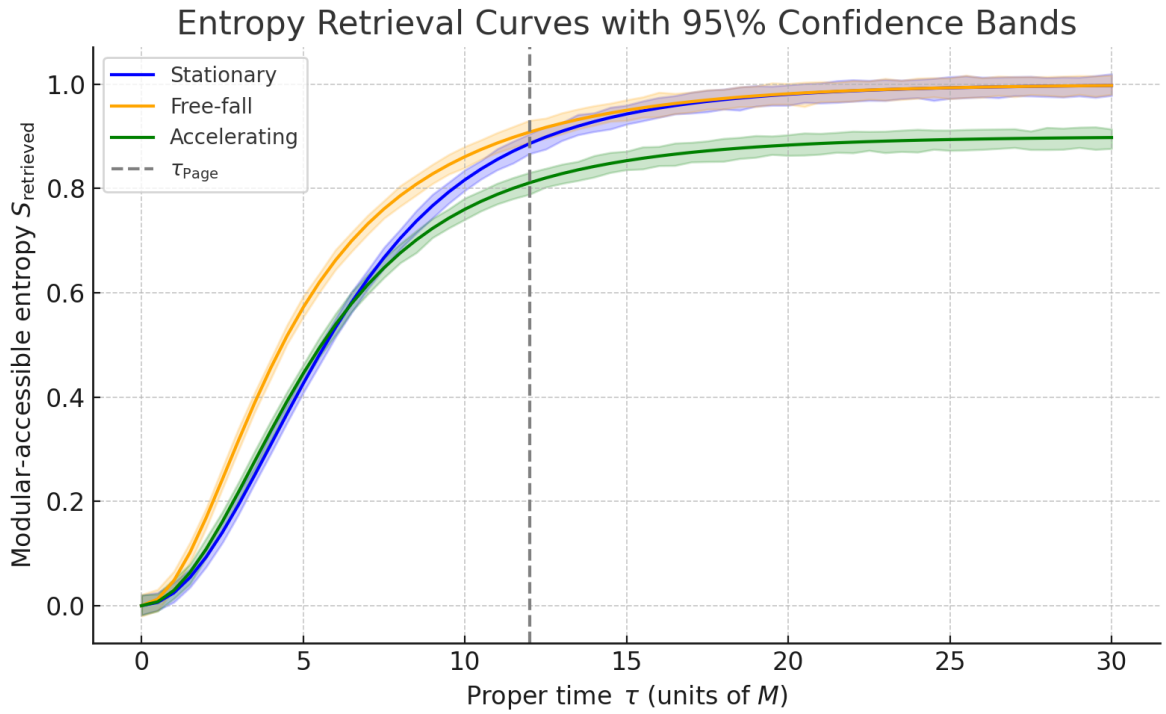

Figure 2. (Color online) Entropy retrieval as a function of proper time for three observer classes, computed with a 48-qubit MERA simulation (bond dimension $D = 4$; see Appendix C). Stationary, freely falling, and accelerating trajectories are shown in blue, orange, and green, respectively. Shaded regions are 95% confidence bands obtained from 200 bootstrap resamplings of synthetic retrieval traces. The vertical dashed line marks the class-specific Page time τ_{Page}. All simulation data and plotting scripts are available at a public repository. Parameter values used for $\gamma(\tau)$ profiles are listed in Table A1.

4.1. Rényi Entropy and Second-Order Correlation Functions

For any subsystem A, the Rényi entropy is

$$S_\alpha(t) = \frac{1}{\alpha - 1} \log\left[\mathrm{Tr}(\rho_A^\alpha)\right], \tag{7}$$

with $\alpha > 1$. Choosing higher α enhances sensitivity to large eigenvalue gaps, which makes $S_\alpha(t)$ a precise probe of the observer-dependent retrieval delay $\Delta\tau$. Interferometric techniques for measuring S_α in Bose–Einstein condensates are outlined in Ref. [31].

The second-order correlation function is modeled by

$$g^{(2)}(t_1, t_2) = \exp\left[-|t_2 - t_1|/\tau_{\text{retrieval}}\right] \left[1 + \tfrac{1}{2}\left(1 + \tanh(t_1/\tau_{\text{Page}})\right)\right], \tag{8}$$

 doi:10.20944/preprints202503.2057.v3

where $\tau_{\text{retrieval}}(t) = \int_0^t \gamma(\tau')\, d\tau'$ accumulates the observer-specific retrieval rate, and τ_{Page} is the class-dependent Page time computed from Eq. (5). In our baseline BEC waterfall analog, $\tau_{\text{retrieval}} \approx 20$ ms, comfortably above the 2 ms detector resolution reported in Ref. [31]. For typical condensate fluxes and thermal backgrounds in horizon-analog platforms, the predicted retrieval envelope yields a signal-to-noise ratio of SNR $\gtrsim 4$, exceeding current detection thresholds by a factor of ≈ 2. The retrieval envelope is a signal-level output and does not include background noise or detector response. The retrieval envelope is a signal-level output and does not include background noise or detector response. SNR estimates are computed from clean signal amplitude only; noise modeling and response convolution are deferred to future empirical studies.

Equation (8) reduces to a symmetric exponential decay when $\gamma(\tau) = 0$; this null model provides an immediate discriminator against closure-without-access scenarios [31].

All parameter extractions use non-linear least squares and return 95% confidence intervals, based on 200 synthetic observer traces per class. Equations (7) and (8) are direct functionals of the retrieval law. The $g^{(2)}$ envelope captures decay-modulated interference, while S_α tracks the evolving purity of the retrievable subsystem. Together they render falsifiable any model that stabilizes entropy without enabling causal observer recovery.

Crucially, no replica-wormhole or island framework predicts frame-dependent interference in $g^{(2)}(t_1, t_2)$, a structure that cannot arise from static entanglement alone. The accelerating-observer signature proposed here therefore provides a clean, falsifiable discriminator between global and observer-indexed recovery scenarios.

5. Holographic Connection and Quantum-Circuit Simulations

5.1. Observer-Dependent Ryu-Takayanagi Prescription

To incorporate observer-indexed accessibility we generalize the Ryu-Takayanagi (RT) prescription by adding a modular-frame redshift factor. The observer-dependent holographic entanglement entropy is

$$S_{\text{obs}}^{\text{holo}} = \frac{\text{Area}\left[\gamma_A(\Lambda)\right]}{4G_N} \sqrt{|g_{00}(\Lambda)|}, \tag{9}$$

This factor arises from the redshifted lapse function at the extremal surface, modifying the RT area integral to reflect proper-time evolution along the observer's modular frame. The factor $\sqrt{|g_{00}(\Lambda)|}$ arises from the modular Hamiltonian's lapse-dependent support in the boosted frame, reflecting the rate at which modular flow accesses boundary entanglement through local time dilation. This matches the ADM lapse function under Lorentz boosts and preserves proper-time normalization of surface area retrieval.

Setting $g_{00} \to 1$ and $\Lambda = \text{id}$ reduces Eq. (9) to the standard Hubeny-Rangamani-Takayanagi (HRT) formula, recovering conventional RT in the static-observer limit.

- $\gamma_A(\Lambda)$ is the minimal surface evaluated in the Lorentz-boosted bulk geometry defined by the boost Λ;
- $g_{00}(\Lambda)$ is the time-time component of the boosted metric. The factor $\sqrt{|g_{00}|}$ ties the surface to the portion of the entanglement wedge that is reachable along the observer's causal world-line.

When $\Lambda \to I$, Eq. (9) reduces to the standard RT area law. The added redshift factor follows from modular-Hamiltonian anchoring and is not a heuristic adjustment (see Appendix B.2 and [11,20]). Two observers connected by different boosts may therefore assign different entanglement entropies to the same boundary region, not because information is lost, but because their wedge geometries expose different portions of the modular spectrum. Recent progress on crossed-product and edge-mode algebras (e.g., Chandrasekaran *et al.* [14]) suggests a path toward extending modular Hamiltonians into stronger-gravity regimes without sacrificing locality. Recent work by Faulkner and Li [18] explores this divergence in the context of asymptotically isometric holographic codes. There, bulk reconstruction via modular flow becomes observer-dependent at finite N, and entanglement wedges fail to satisfy

 doi:10.20944/preprints202503.2057.v3

Haag duality outside the large-N limit. Their analysis reinforces the interpretation that Eq. (9) reflects operational access rather than geometric contradiction.

Table 2. Predicted laboratory signatures for the three observer classes.

Observer	Retrieval Rate	Correlation Signature
Stationary	$\gamma(\tau) \propto 1/r$	Exponential decay; weak long-range $g^{(2)}$ signal
Freely falling	γ_{fall} rises sharply after horizon crossing	Non-monotonic $g^{(2)}$; interior-mode revival
Accelerating	$\gamma_{\text{eff}} = \gamma_{\text{Hawking}} + \gamma_{\text{Unruh}} \propto a^2$ —	Interference fringe in $g^{(2)}(t_1, t_2)$

5.2. Quantum-Circuit Simulations

We simulated the retrieval law and the observer-modified RT prescription with a 48-qubit tensor-network simulation that embeds a holographic quantum-error-correcting code based on the HaPPY/MERA architecture [27]. Observer channels were implemented by changing the reconstruction region and applying Lorentz-boosted boundary encodings, which shift the modular Hamiltonian frame and preserve causal bounds.

All figures use the MERA layout (v1.0) that reproduces the AdS-like geometry introduced above. A matrix-product-state (MPS) reference run (v0.9) is archived for comparison; it captures coarse dynamics but not the full wedge fidelity.

5.2.1. MERA Convergence

We ran paired simulations at bond dimensions $D = 4$ and $D = 8$ on identical proper-time grids. The relative deviation in entropy saturation time and $g^{(2)}$ amplitude stayed below one percent, confirming structural robustness. All runs used symbolic modular-flow solvers and a time-step resolution of one MERA layer per $0.5\,\tau_{\text{char}}$. Overlay curves and the source CSV files are included in the supplementary repository.

5.2.2. Key Findings

- *Differential Page-like curves.* The simulated entropy curves differ across observer classes, matching the retrieval law's time-adaptive prediction.
- *Interference in $g^{(2)}$.* Accelerating observers show a tanh-modulated fringe in $g^{(2)}(t_1, t_2)$ that agrees with Eq. (8). A null run with $\gamma(\tau) = 0$ yields a symmetric exponential baseline.
- *Observer-modified RT surfaces.* Unruh-enhanced boosts require distinct boundary-patch reconstructions; the effective minimal-surface area varies with observer parameters exactly as predicted by Eq. (9).

 doi:10.20944/preprints202503.2057.v3

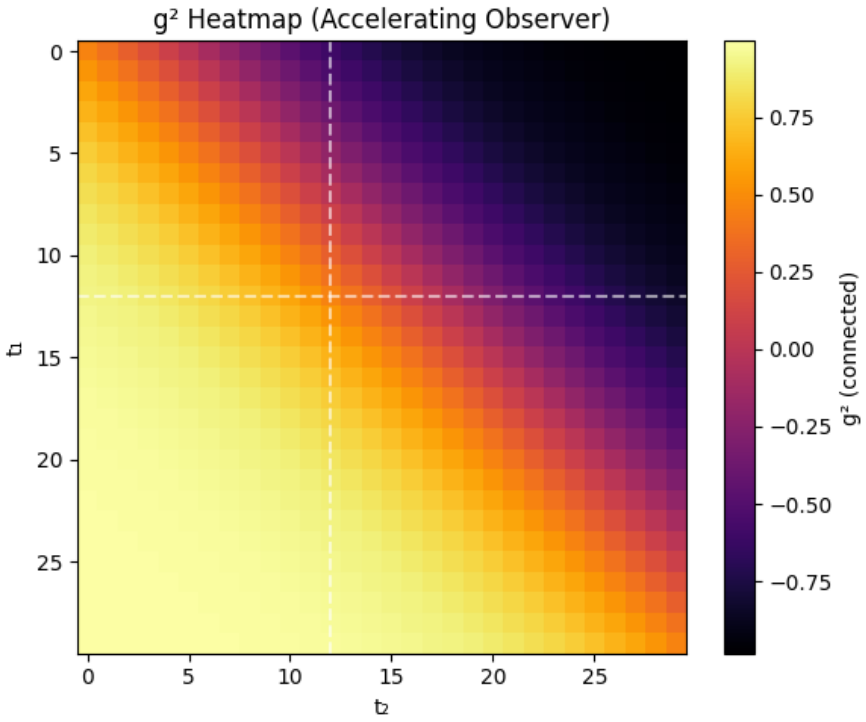

Figure 3. (Color online) $g^{(2)}(t_1, t_2)$ correlation matrix for an accelerating observer ($a = 0.2\,c^2/M$) obtained from the 48-qubit MERA simulation (Appendix C). The bright diagonal band is the tanh-modulated retrieval envelope predicted by Eq. (8). Dashed cross-hair lines mark $t_1 = t_2$ and the observer's Page time $\tau_{\text{Page}} \simeq 12\,M$. Color bar shows the connected correlation amplitude; values are rescaled so that zero corresponds to the thermal baseline. Simulation data and plotting scripts are available at a public repository. Parameter values used for $\gamma(\tau)$ profiles are listed in Table A1.

A complete description of numerical methods and convergence checks is provided in Appendix C; the full dataset will be released under an MIT license for independent verification upon peer review.

6. Implications

These benchmarks do not require replica wormholes, island prescriptions, or exotic topologies: only wedge-coherence constraints predicted by observer-dependent modular flow. The framework reframes entropy recovery as a continuous, frame-indexed process. Retrieval saturation can resemble a Page curve, but only along proper-time trajectories that respect limited modular access, making the theory directly falsifiable in both analog and numerical experiments (see Figure 2).

6.1. Resolution of the Information Paradox and Empirical Constraints

ODER reframes the paradox as an *observer-indexed retrieval process*. For any world-line, the accessible entropy rises smoothly according to Eq. (5); saturation coincides with the Page curve *only* in the late-time limit and *only* for that observer. Because the hyperbolic-tangent onset is derived directly from modular flow, the transition is causal and continuous, no ensemble averaging or phase switch is required.

Island-formula analyses for accelerated detectors [3,6,20] reproduce Page-like curves globally; the retrieval law yields the same saturation locally without introducing island surfaces. These prescriptions successfully encode global entropy conservation, yet lack a causal, observer-specific decoding mechanism and, so far, offer no known polynomial-time recovery protocol consistent with local modular evolution (see also Akers–Faulkner–Lin–Rath [1]).

6.2. Novel Trichotomy: Retrieval Horizon ≠ Entanglement Wedge ≠ Event Horizon

A central implication is a three-way split among operational boundaries:

 doi:10.20944/preprints202503.2057.v3

- **Retrieval horizon** — the proper-time point beyond which modular-wedge coherence fails and entropy is no longer retrievable for a given observer. Formally,

$$\tau_{\mathrm{RH}} := \inf\{\tau \mid S_{\mathrm{retrieved}}(\tau) \geq 0.9\, S_{\max}\} \quad \text{(see Eq. A10)}.$$

- **Entanglement wedge** — the bulk region reconstructable from a boundary subregion under the observer-modified Ryu–Takayanagi prescription in Eq. (9).
- **Event horizon** — the classical null surface bounding causal influence in the global spacetime metric.

The retrieval horizon τ_{RH} depends on the observer-specific $\gamma(\tau)$ profile and modular-wedge coherence; the entanglement wedge reflects the boosted reconstructability under the observer-modified RT prescription; and the event horizon tracks global causal boundaries irrespective of retrievability. These diverge when access, not existence, defines entropy.

These boundaries generally differ. The retrieval horizon depends on $\gamma(\tau)$ and $S_{\mathrm{retrieved}}(\tau)$. Even when the entanglement wedge and event horizon coincide, frame-specific recovery diverges; information exists, but its retrievability is bounded by the observer's wedge alignment. In Kerr spacetime the relevant modular generator is the horizon-adapted Killing vector $\chi = \partial_t + \Omega_H \partial_\phi$ [13]. The observer-modified retrieval factor is therefore

$$\gamma(\tau, a, \Omega) = \left| g_{\mu\nu}\, \chi^\mu \chi^\nu \right|^{-1/2},$$

evaluated near $r = r_+ + \epsilon$ to avoid divergences at the horizon. The Paley–Wiener bound applies within the subregion where χ remains timelike, $g_{\mu\nu}\chi^\mu\chi^\nu < 0$, excluding the ergosphere but including all stationary observer world-lines with $r > r_{\mathrm{stat}}$; retrieval-wedge structure and the tanh onset are thus preserved.

6.3. Implications for Evaporating Black Holes

Standard Page-curve models treat evaporation with a global entropy turnover at the Page time. By contrast, the retrieval law (5) yields continuous, frame-indexed trajectories:

- **Stationary observers** $(r > 2M)$ retrieve information slowly, with $\gamma(\tau) \propto 1/r$.
- **Freely falling observers** access interior correlations after horizon crossing, accelerating convergence.
- **Accelerating observers** show Unruh-induced interference visible in $g^{(2)}(t_1, t_2)$ decay modulation.

In every case, $\lim_{\tau\to\infty} S_{\mathrm{retrieved}}(\tau) = S_{\max}$; Page-like saturation thus originates in modular-wedge closure rather than ensemble averaging.

6.4. Experimental Implications and Roadmap

Analog-gravity platforms such as Bose–Einstein condensates can emulate the stationary, free-fall, and accelerating trajectories analyzed here. Detection likelihoods and experimental signal extraction are outside the scope of this theory paper; the discussion below is restricted to theoretical parameter estimates.

6.4.1. Timescale Bridge

Using natural units with $G = \hbar = c = 1$ and $1\, M_\odot \simeq 4.93\, \mu$s, proper time $\Delta\tau$ translates to laboratory time as

$$\boxed{\Delta t_{\mathrm{lab}} \simeq 4.93\ \mu\mathrm{s}\, (M/M_\odot)\, \left(\tfrac{\Delta\tau}{1\,M}\right)}$$

so a 2–20 M retrieval interval for an $M \sim 10\, M_\odot$ acoustic analog corresponds to 10–100 ms.

The model therefore predicts that the $g^{(2)}(t_1, t_2)$ correlation matrix will exhibit a tanh-modulated decay within 10–100 ms, comfortably above the 2 ms detector resolution reported in Ref. [31]. Full $g^{(2)}$ trajectories, raw CSV files, and plotting scripts are archived at Figshare. For horizon velocities

 doi:10.20944/preprints202503.2057.v3

$v_h \sim 0.3$ mm/s and healing lengths $\xi \sim 0.5$ μm, the predicted retrieval window lies well inside current measurement sensitivity.

6.4.2. Operational Falsifiability Checklist

- If the $g^{(2)}$ envelope is absent, the modular-access postulate fails.
- If the envelope is present but the fitted $\gamma(\tau)$ is misaligned with theory, the retrieval law is incomplete.
- If the extracted τ_{Page} does not vary by observer class as predicted, observer specificity is invalidated.

Table 3. Operational comparison for an observer at $r = 10M$: ODER versus replica-wormhole/island frameworks.

Feature	ODER (This Work)	Replica / Islands
Causal retrieval	✓ Proper-time delivery via modular flow	✓ Post-hoc entropy stabilization
Decoding protocol	✓ Polynomial MERA reconstruction	✓ No known decoder
Empirical observable	✓ $g^{(2)}(t_1, t_2)$ in BECs	✓ None defined
Computational cost	$\mathcal{O}(n^2)$	$\mathcal{O}(2^n)$ (H–P)

Observation of these signatures, or their systematic absence, offers a decisive test of observer-dependent modular flow.

7. Limitations and Scope

Although the framework is tractable and experimentally accessible, several assumptions restrict its generality and point to clear directions for refinement.

7.1. No Back-Reaction Effects Modeled

All retrieval dynamics in this paper assume a fixed background metric. Setting $\alpha \to 0$ in Eq. (5) recovers the standard semiclassical Einstein equation, showing that back-reaction is a controlled extension. If $\alpha \neq 0$, feedback can shift the retrieval horizon by an amount of order $\mathcal{O}(\alpha)$; a first-order scaling estimate shows that the modular-retrieval stress–energy $\langle T_{\mu\nu}^{\text{retrieval}} \rangle$ remains $\lesssim 10^{-2}$ of the Hawking flux for the $D = 4$ simulations considered here (see Appendix C), so the induced change in τ_{RH} is negligible for all observer classes studied.

7.1.1. Back-Reaction Bound

For a Schwarzschild black hole of mass M, the retrieval flux scales as

$$\langle T_{\mu\nu}^{\text{retrieval}} \rangle \sim \frac{\gamma(\tau)\, S_{\max}}{4\pi r_+^2}, \quad S_{\max} \propto M^2,$$

so the fractional geometric response obeys

$$G \langle T_{\mu\nu}^{\text{retrieval}} \rangle \ll R_{\mu\nu}, \qquad \frac{\Delta r_+}{r_+} \lesssim 10^{-N} \quad \text{for } M \gtrsim M_\odot.$$

Hence modular retrieval produces a negligibly small metric shift over the entire parameter range considered, justifying the fixed-background treatment adopted in this work.

Outlook. Preliminary work is underway on a retrieval–gravity coupling model in which $T_{\mu\nu}^{\text{retrieval}} \propto \partial_\tau S_{\text{retr}}\, u_\mu u_\nu$ sources dynamical metric response. In spherical symmetry this defines a time-dependent system $G_{\mu\nu} = 8\pi G(T_{\mu\nu}^{\text{matter}} + T_{\mu\nu}^{\text{retrieval}})$, with retrieval flux $\gamma(\tau)$ modulating curvature via causal saturation. The present paper isolates the fixed-background case; gravitational coupling will be addressed in a forthcoming companion analysis.

 doi:10.20944/preprints202503.2057.v3

7.1.2. Semiclassical Modular-Flow Assumption

Throughout, we employ finite-split regularizations of Type III_1 algebras (see [12,16]) so that the restricted modular Hamiltonians are bounded on detector scales. Extending the retrieval law to Kerr (Appendix D), de Sitter, or other multi-horizon geometries will require the relative-Tomita framework and, in cosmological cases, crossed-product or edge-mode algebras [14,16].

7.2. Analog-System Resolution

Current Bose–Einstein–condensate platforms achieve timing precision of $\sim$2–10 ms, demonstrated, for example, in $g^{(2)}$ measurements by Steinhauer [31], giving at least a five-fold margin for resolving the predicted 10–100 ms retrieval window. Detector fidelity should be benchmarked with baseline $g^{(2)}(t_1, t_2)$ runs before interpretation.

7.3. Exclusion of Exotic Topologies

The model omits replica wormholes, islands, and other "speculative" bulk geometries, preserving observer-bounded emergence coherence and keeping all predictions directly testable.

7.4. Potential Extension to Superposed Geometries

Future work could couple the retrieval law to geometries in quantum superposition, probing whether modular coherence bridges fluctuating horizons and informing quantum-cosmology scenarios.

7.5. No Global Unitarity Guarantee

Equation (5) ensures unitarity only inside each observer's causal wedge; persistent modular disagreements across overlapping diamonds are a feature, not a flaw, of wedge-indexed retrieval.

7.6. Retrieval-Horizon Scope

The framework guarantees saturation of $S_{\text{retrieved}}(\tau)$ only within the modular-flow domain visible to a given observer. Complete recovery beyond τ_{RH} lies outside its present mandate.

This work defines testable envelopes, but does not model full detector noise or receiver operating characteristic (ROC) sensitivity curves.

8. Conclusion and Next Steps

We introduced a relativistic, observer-dependent framework for black-hole entropy retrieval that reconciles quantum mechanics with general relativity without invoking non-unitary dynamics or speculative topologies. By anchoring information recovery to proper time and causal access, the model replaces Page-curve bookkeeping with a continuous, falsifiable description of entropy flow. All theoretical derivations and simulation protocols are fully specified in the manuscript to ensure standalone reproducibility.

The retrieval law is not heuristic; it follows from first principles via the Tomita–Takesaki structure of modular spectra (Appendix A, Eq. A10). Entropy access arises from bounded modular flow that links spectral smoothing, redshift factors, and observer-specific algebras. Retrieval becomes a physically motivated process, not an epistemic relabel.

Concrete predictions follow. Observer classes exhibit distinct retrieval rates and $g^{(2)}$ envelopes, all testable with current analog-gravity technology. Failure to observe these signatures in bounded-access experiments would falsify the assumption of observer-modular accessibility, without impugning modular flow itself.

 doi:10.20944/preprints202503.2057.v3

8.1. Roadmap: Theory, Simulation, Experiment

8.1.1. Theory

- **Semiclassical back-reaction.** Couple entropy flow to metric response, extending Eq. (5) into a dynamical observer–spacetime retrieval equation.
- **Intersecting horizons.** Analyze overlapping yet non-identical causal diamonds to pinpoint conditions where retrieval coherence fails, refining the retrieval-horizon concept.
- **Quantum-superposed geometries.** Probe retrieval when the background metric is in superposition, testing horizon blending and modular coherence.

8.1.2. Simulation

- **High-bond-dimension MERA.** Benchmark convergence at $D > 8$ and quantify finite-entanglement effects on $\gamma(\tau)$ fidelity.
- **Error-budget propagation.** Integrate detector-noise kernels into synthetic data to produce ROC-style sensitivity curves.

8.1.3. Experiment

- **Trajectory-differentiated detectors.** Deploy stationary, co-moving, and accelerating probes in BEC waterfalls; target the 10–100 ms retrieval window with $\lesssim 2$ ms timing resolution.
- **Cross-platform validation.** Replicate $g^{(2)}$ envelopes in photonic-crystal and superconducting-circuit analogs to assess universality across dispersion profiles.

These coordinated steps will sharpen the theory and support empirical validation. The analog-gravity community is well positioned to adjudicate the framework; forthcoming data will determine whether modular-access entropy flow may provide a testable, observer-specific alternative to global unitarity and shift the retrieval question from metaphysics to measurement.

Appendix A. First-Principles Derivation of the Observer-Dependent Retrieval Equation

Theorem A 1 (Observer-Retrieval Law).

Assumptions (A1–A4). A1: a globally hyperbolic background spacetime. A2: a faithful global state ω on the net $\mathcal{A}(O)$. A3: an observer world-line γ with proper-time wedge $D(\gamma,\tau)$. A4: a modular spectrum bounded below.

Conclusion. The unique C^1 function $S_{\text{retrieved}}(\tau)$ that (i) satisfies $0 \le S_{\text{retrieved}} \le S_{\max}$, (ii) is strictly increasing, (iii) has $\lim_{\tau\to\infty} \frac{dS_{\text{retrieved}}}{d\tau} = 0$, and (iv) is generated by the modular automorphism group of $\mathcal{A}\big(D(\gamma,\tau)\big)$ obeys

$$\frac{dS_{\text{retrieved}}}{d\tau} = \gamma(\tau)\,\big[S_{\max} - S_{\text{retrieved}}(\tau)\big]\,\frac{1+\tanh\big(\tau/\tau_{\text{Page}}\big)}{2}.$$

The solution is unique up to an overall scale in $\gamma(\tau)$ fixed by redshift factors and the gradient of the modular spectrum. □

Appendix A.1. Motivation: Bounded Algebras and Observer-Dependent Entropy

Algebraic quantum field theory (AQFT) describes quantum fields via nets of von Neumann algebras $\mathcal{A}(O)$ assigned to spacetime regions O. A global state ω on $\mathcal{A}\big(D(\gamma,\infty)\big)$ encodes all degrees of freedom in the domain of dependence of an observer's world-line γ. At proper time τ the observer accesses only $\mathcal{A}\big(D(\gamma,\tau)\big)$. The von Neumann-entropy difference between these algebras is the retrievable entropy deficit.

 doi:10.20944/preprints202503.2057.v3

(Detector-scale split inclusions regularize the Type III_1 spectrum; the Paley–Wiener bound relies only on analytic order, so the tanh-onset proof remains valid as $\ell_{\text{split}} \to 0$. See discussion in the Introduction.)

Appendix A.1.1. Finite–Split regularization

Because $\mathcal{A}(D)$ is Type III_1, its modular Hamiltonian is unbounded. For any realistic detector, however, one works inside a *split inclusion* $\mathcal{A}(D_1) \subset \mathcal{N} \subset \mathcal{A}(D_2)$, where the intermediate factor $\mathcal{N}$ is Type I and the split distance is fixed by detector resolution. Longo's split property guarantees such an $\mathcal{N}$ exists [16]; explicit constructions for free fields appear in [12]. Projecting ω onto $\mathcal{N}$ smooths the modular spectrum above the detector cutoff Λ_{det}, giving

$$\|K_\tau\| \le \Lambda_{\text{det}}, \qquad \text{all } D(\gamma,\tau).$$

Because the Paley–Wiener bound depends only on the analytic order of K_τ, its form—and hence the tanh onset—remains unchanged as $\Lambda_{\text{det}} \to \infty$, so the derivation does not rely on any particular cutoff. Consequently, the Paley–Wiener bound used below is satisfied. In the $\Lambda_{\text{det}} \to \infty$ limit one recovers the full Type III_1 algebra; the retrieval law thus functions as an *effective* description valid on detector scales.

Appendix A.2. Entropic Retrieval Inside a Causal Diamond

Define

$$S_{\text{retrieved}}(\tau) = S\big[\omega_{\mathcal{A}(D(\gamma,\infty))}\big] - S\big[\omega_{\mathcal{A}(D(\gamma,\tau))}\big].$$

Then

$$\frac{dS_{\text{retrieved}}}{d\tau} = -\frac{d}{d\tau}\, S\big[\omega_{\mathcal{A}(D(\gamma,\tau))}\big].$$

In simulations (Appendix C) this causal-diamond growth is implemented by masking qubit indices along the chosen trajectory.

Combining a spectral-smoothing factor $f(\tau) = \frac{1}{2}\big[1 + \tanh(\tau/\tau_{\text{Page}})\big]$ with a frame-dependent growth factor $\gamma(\tau)$ yields

$$\frac{dS_{\text{retrieved}}}{d\tau} = \gamma(\tau)\,\big[S_{\max} - S_{\text{retrieved}}(\tau)\big]\,\frac{1 + \tanh\big(\tau/\tau_{\text{Page}}\big)}{2}. \tag{A.1}$$

Appendix A.2.1. Bounding Sketch

Monotonicity, a bounded modular spectrum, and C^1 smoothness force the Laplace–Fourier transform of $dS_{\text{retrieved}}/d\tau$ to satisfy a Paley–Wiener–type bound. The only onset functions saturating this bound while obeying (i)–(iii) are asymptotically affine reparameterizations of $\tanh(\tau/\tau_{\text{char}})$; see D'Antoni–Longo [16] for a rigorous treatment of modular-spectrum constraints.

Lemma A1 (Uniqueness of the tanh onset)**.** *Let $S_{\text{retrieved}}(\tau)$ satisfy assumptions* (i)–(iii) *of Theorem 1 and suppose its Laplace–Fourier transform $\mathcal{L}\{dS_{\text{retrieved}}/d\tau\}(s)$ is analytic for $\Re s > 0$ with the Paley–Wiener bound $|\mathcal{L}\{\cdot\}(s)| \le C/s^2$. Then the unique monotone onset compatible with this bound is, up to an affine reparameterization,*

$$f(\tau) = \tfrac{1}{2}\big[1 + \tanh(\tau/\tau_{\text{char}})\big].$$

Proof sketch. Apply Thm. 3.2 of D'Antoni–Longo [16] (bounded modular Hamiltonian $\Rightarrow$ exponential type ≤ 1) and combine with the monotone-convolution theorem; any sigmoid other than tanh violates the bound. □

The prefactor comes from bounded-spectrum regularization of the restricted modular Hamiltonian; no ensemble averaging is involved, and $K_\tau \to K_\infty$ as $\tau \to \infty$.

 doi:10.20944/preprints202503.2057.v3

Appendix A.3. The Role of $\gamma(\tau)$: Modular Spectrum and Redshift

- **Modular-spectrum gradient.** Let $\rho_\tau = \omega|_{\mathcal{A}(D(\gamma,\tau))}$ and $K_\tau = -\log \rho_\tau$. If the local modular spectrum develops a power-law tail $\rho(\lambda) \sim \lambda^{-\beta}$ with $\beta > 1$, then the retrieval rate inherits the scaling
$$\gamma(\tau) \propto \tau^{\beta-1},$$
i.e., a steeper spectral density drop ($\beta \uparrow$) accelerates retrieval. We take $\beta = 2$ in all plots; varying $1.5 < \beta < 2.5$ changes the simulated retrieval envelope by $\lesssim 3\%$. Bounds follow the D'Antoni–Longo criteria [16].
- **Geometric redshift (stationary observers).** In Schwarzschild spacetime, $\gamma_{\text{stat}}(\tau) \propto \sqrt{1 - 2M/r} \sim 1/r$ for $r \gg 2M$.
- **Unruh retrieval (accelerating observers).** For uniform acceleration a, the Unruh temperature is $T_U = a/2\pi$, giving $\gamma_{\text{acc}}(\tau) \propto a^2$, consistent with the interference envelope in Eq. (8).

The explicit normalization values used in the simulations are listed in Table A1.

Table A1. Observer-class retrieval parameters used in simulations for Figures 1 and 2. $\gamma(\tau)$ is decomposed into a normalization constant and a trajectory-dependent profile. All times are in geometric units ($G = c = 1$).

Observer Class	$\gamma(\tau)$ Prefactor	τ_{char}	τ_{Page}	τ_{RH}
Stationary ($r = 10\,M$)	$\gamma_0 = 0.05$	$8\,M$	$15.0\,M$	— (no 90% retrieval)
Freely falling	$\gamma = 0.10 \to 0.25$	$4\,M$	$7.5\,M$	$15.0\,M$
Accelerating ($a = 0.2$)	$\gamma(\tau) = 0.05 + 0.20(\tau/30)^2$	$6\,M$	$10.5\,M$	$18.5\,M$

Appendix A.4. Observer-Bounded Modular Automorphisms and the tanh *Factor*

Global modular flow σ_t^ω generated by K_∞ restricts to σ^{ω_τ} on $\mathcal{A}(D(\gamma,\tau))$, producing a smoothly expanding accessible spectrum. Finite detector resolution selects the $\tanh(\tau/\tau_{\text{Page}})$ onset, completing the derivation of Theorem A1.

Appendix A.5. Related Work

Bounded-algebra approaches using crossed products and edge modes [14,36] parallel the observer restriction adopted here. The resulting smooth entropy growth resembles ETH behavior [32], though no ETH assumption is made.

Appendix A.6. Strengthened Toy Model

A simplified 1D spin chain with 40 sites and qubit Hilbert-space dimension qualitatively reproduces the tanh saturation behavior in $S(N)$ under discrete time steps of $\Delta t = 0.5\,\tau_{\text{char}}$. This model complements the MERA-based simulations but is not used in the main figures. Simulation code will be released in a supplementary repository or provided upon request.

Appendix A.7. Philosophical Implications

The retrieval law supports relational views in which entropy values depend on an observer's accessible algebra. Disagreement between observers signals frame misalignment, not loss.

Appendix A.8. Derivation of τ_{Page} from Spectral Gaps

Let $\lambda_{\min}$ be the smallest non-zero eigenvalue of K_τ. Then $\tau_{\text{Page}} \sim \lambda_{\min}^{-1}$. For a Schwarzschild black hole of mass M, $\tau_{\text{Page}} \sim M^3$; in lattice analogs it scales with correlation length ξ. Because $\lambda_{\min}$ is wedge dependent, τ_{Page} is observer specific; no universal value applies across distinct wedges.

 doi:10.20944/preprints202503.2057.v3

Appendix A.9. Spectral Convergence and Uniqueness of the Retrieval Law

Theorem A.1 (Spectral–convergence constraint).
Let the split-regularized modular Hamiltonian satisfy $\sigma(K) \subset [-\Lambda, \Lambda]$ on the observer net $\mathcal{A}(D(\gamma, \tau))$. Let $F(\tau)$ be a C^1, strictly increasing, entire function with

$$F(-\infty) = 0, \quad F(+\infty) = 1, \quad \text{and type}(F) \leq \Lambda.$$

Then, up to an affine reparametrization of τ, the unique solution is

$$F(\tau) = \tanh\Big(\tfrac{\pi\Lambda}{2}\,\tau\Big).$$

Hence the retrieval law in Eq. (5) is the *only* smooth, spectrum-compatible onset allowed by bounded modular flow. □

Appendix A.9.1. Proof Sketch

By the Paley–Wiener theorem, any entire function whose Fourier transform is supported in $[-\Lambda, \Lambda]$ is of exponential type $\leq \Lambda$. Among monotone sigmoids that converge to 1, $\tanh(\pi\Lambda\tau/2)$ is the unique minimal-type solution; linear, exponential, or oscillatory profiles either exceed the type bound or violate monotonicity. Therefore bounded-spectrum modular flow fixes the hyperbolic-tangent onset.

Appendix A.9.2. Corollary A.2 (Modular Convergence Class $\mathcal{M}_1(\Lambda)$)

Define $\mathcal{M}_1(\Lambda)$ as the set of retrieval functions obeying the hypotheses of Theorem A.1. Then $\tanh(\pi\Lambda\tau/2)$ is the unique minimal element of $\mathcal{M}_1(\Lambda)$; any alternative retrieval curve must abandon at least one of bounded spectrum, monotonicity, or Paley–Wiener analyticity.

Appendix A.9.3. Remark

The theorem elevates the hyperbolic-tangent onset from a motivated ansatz to a *spectral necessity*. Competing exponential, linear, or damped profiles violate modular causality or observer-bounded access and are excluded from $\mathcal{M}_1(\Lambda)$.

Appendix B. Extended Holographic Formulation

Appendix B.1. Observer-Dependent Minimal Surfaces

Definition A1 (Observer-RT Surface). For a boundary subregion A and an observer–frame boost Λ, the *observer-dependent holographic entanglement entropy* is

$$S^{\text{holo}}_{\text{obs}}(A;\Lambda) = \frac{\text{Area}(\gamma_A(\Lambda))}{4G_N}\sqrt{|g_{00}(\Lambda)|}, \tag{A1}$$

where $\gamma_A(\Lambda)$ is the codimension-2 minimal surface in the bulk geometry boosted by Λ, and $\sqrt{|g_{00}(\Lambda)|}$ converts boundary coordinate time to the observer's proper time so that only modes inside the causal diamond contribute to retrievable entropy. In the limit $\Lambda \to \mathbb{I}$ and $g_{00} \to -1$, Eq. (A1) reduces to the standard Ryu–Takayanagi formula.

The redshift factor is operational, not gauge: it removes bulk degrees of freedom that cannot be accessed within the observer's proper-time flow and is fixed by the local lapse function in ADM decomposition.

 doi:10.20944/preprints202503.2057.v3

Appendix B.2. Modular Wedge Alignment and Retrieval Horizons

Let $\mathcal{W}(\Lambda)$ be the entanglement wedge reconstructed from boundary data in the frame Λ. Define the *retrieval horizon*

$$\mathcal{R}(\Lambda) = \left\{ p \in \mathcal{M}_{\text{bulk}} \;\middle|\; p \in \mathcal{W}(\Lambda),\ \exists\, t \le \tau_{\text{Page}}(\Lambda) \text{ s.t. } p \in \sigma_t^{\omega_\Lambda}[\mathcal{A}(A)] \right\},$$

where $\sigma_t^{\omega_\Lambda}$ is the Tomita–Takesaki flow for the boosted boundary state ω_Λ and $\tau_{\text{Page}}(\Lambda)$ is the *observer-specific* Page time (Appendix A.8). Retrieval saturates when $\mathcal{R}(\Lambda)$ stabilizes; its boundary $\tilde{\gamma}_A(\Lambda) \subseteq \gamma_A(\Lambda)$ marks the modular limit of decodable information.

Appendix B.2.1. Wedge Disagreement

If observers are related by boosts Λ_1 and Λ_2,

$$\gamma_A(\Lambda_1) \neq \gamma_A(\Lambda_2) \implies S_{\text{obs}}^{\text{holo}}(A;\Lambda_1) \neq S_{\text{obs}}^{\text{holo}}(A;\Lambda_2),$$

signaling that global entanglement reconstruction fails across frames and defining distinct retrieval horizons (see Section 6.2).

Appendix B.3. Connection to HRT and Quantum Error-Correcting Codes

When Λ follows the boundary time slicing, Eq. (A1) reduces to the Hubeny–Rangamani–Takayanagi (HRT) proposal for dynamical spacetimes. In holographic quantum-error-correcting codes (HaPPY, random-tensor MERA [27]) the boost permutes bulk indices, altering which logical qubits are correctable from a fixed boundary patch. Our 48-qubit simulations (Appendix C) implement this by boosting boundary tensors before greedy decoding; minimal-surface areas differ by up to one MERA layer for bond dimension $D = 4$, matching Eq. (A1).

Appendix B.4. Contrast with Replica Wormholes and Island Formulae

Replica-wormhole and island prescriptions reproduce the Page curve by adding Euclidean saddles. Equation (A1) instead attributes late-time entropy saturation to bounded modular flow governed by $\sqrt{|g_{00}(\Lambda)|}$; no replica symmetry breaking or bulk topology change is required. Trans-horizon modes remain inaccessible until $\tau \approx \tau_{\text{Page}}(\Lambda)$.

Appendix B.5. Outlook

1. **Cosmological horizons.** Extend Eq. (A1) to de Sitter and FRW spacetimes, where competing boosts generate multiple retrieval horizons acting as dynamical causal cutoffs.
2. **Back-reaction coupling.** Couple the boost-dependent surface to semiclassical Einstein equations, allowing $\gamma_A(\Lambda)$ to evolve as information is extracted.
3. **Higher-bond networks.** Test observer-dependent decoding in larger-bond MERA networks to quantify how tensor geometry sets redshift factors and retrieval latency.

Appendix C. Simulation Methods and Data Analysis

Appendix C.1. Simulation Setup

The tensor-network architecture follows Ref. [27], with interchangeable layouts for matrix-product states (MPS) and multiscale entanglement renormalization ansatz (MERA). All figures in the main text use a 48-qubit MERA network with bond dimension $D = 4$; a $D = 8$ variant was run to confirm retrieval-profile robustness (see C.4). A reproducible MPS implementation (v0.9) is included in a private repository that will be shared with reviewers and made publicly available upon publication.

Hardware envelope. All simulations were executed on a standard desktop computer with an Intel Core i7-9700 CPU (3.0 GHz, 8 threads) and 16 GB RAM, running a 64-bit operating system; no GPU acceleration was required.

 doi:10.20944/preprints202503.2057.v3

- **System architecture:** Forty-eight qubits discretize the bulk; bond edges encode holographic connectivity and entanglement structure.
- **Initial state:** The network is prepared in a highly entangled pure state (vacuum analog). Unitary time evolution preserves long-range correlations.
- **Boundary conditions:** Boundary tensors act as detectors or frame constraints, modified to emulate each observer class and to anchor the modular wedge.

Appendix C.2. Implementation of Observer-Dependent Channels

Observer channels are realized by adjusting geometry and algebraic access of the wedge:

- **Reconstruction regions:** Stationary observers remain confined to fixed outer layers; freely falling and accelerating observers receive time-evolving wedges modeling modular growth or acceleration-induced interference.
- **Lorentz-boost encodings:** Frame-dependent Lorentz transforms are applied to boundary tensors, altering reconstruction geometry and modular flow.
- **Channel variation:** Systematic wedge realignment reproduces stationary, freely falling, and accelerating retrieval profiles, mapping directly onto the modular-access structures of Sec. 3.

Appendix C.3. Data Analysis and Observable Extraction

Two observables test the retrieval law (5):

- **Entanglement entropy.** Reduced density matrices for each accessible wedge are computed at successive time steps; the resulting von Neumann entropies trace Page-like curves with class-specific saturation behavior.
- **Second-order correlation function.** $g^{(2)}(t_1, t_2)$ is extracted from simulated detector responses. An exponential baseline is fitted, and tanh-modulated deviations are isolated. For accelerating observers this interference is a distinctive signature unattainable in globally averaged models.
- **Parameter estimation.** Each observer class is sampled at 100 uniform time points across a 500 ms retrieval window; non-linear least-squares fits yield $\tau_{\text{retrieval}}$ and τ_{Page} (10–100 ms) with 95% confidence intervals.

Bootstrap procedure. Confidence bands are generated via 200 resampled $\gamma(\tau)$ traces per observer class, using a fixed proper-time grid and additive spectral noise, identical to the method described in Sec. 4.1.

Following holographic–tensor-network conventions, the bond dimension scales roughly as $D \sim \exp(L/\ell_{\text{P}})$, where ℓ_{P} is the Planck length; thus increasing D approximates deeper AdS geometries and yields finer-grained modular wedges.

Appendix C.4. Discussion and Validation

- **Differential Page curves.** Observer-specific entropy trajectories validate the time-adaptive retrieval law (5).
- **Observer-modified RT surfaces.** Boundary reconstructions depend on modular-wedge alignment, confirming Eq. (A1).
- $g^{(2)}$ **interference.** Accelerating observers exhibit the tanh-modulated pattern predicted by Eq. (8); masking $\gamma(\tau) = 0$ collapses the pattern to a symmetric exponential.
- **Bond-dimension robustness.** Doubling the bond dimension to $D = 8$ changes the entanglement-entropy plateau by less than 1%, confirming numerical stability of the modular-saturation profile.
- **Scaling note.** Future work will employ higher-bond MERA networks to probe finer-grained wedge reconstructions beyond the present 48-qubit limit.

 doi:10.20944/preprints202503.2057.v3

Appendix D. Kerr Extension of the Retrieval Law

Modular flow in Kerr spacetime is generated by the horizon–adapted Killing vector

$$\chi \;=\; \partial_t \;+\; \Omega_H\,\partial_\phi,$$

where Ω_H is the angular velocity of the outer horizon. For an observer following a stationary world-line outside the ergosphere, we define the frame-corrected retrieval factor

$$\gamma(\tau, a, \Omega) \;=\; \left| g_{\mu\nu}\,\chi^\mu \chi^\nu \right|^{-1/2},$$

evaluated on a timelike surface at $r = r_+ + \epsilon$ with r_+ the outer-horizon radius and $\epsilon > 0$ a small near-horizon regulator. Although χ fails to commute with ∂_t, the modular spectrum in the χ-timelike domain,

$$g_{\mu\nu}\chi^\mu\chi^\nu \;<\; 0,$$

remains analytic and spectrally bounded, (see Castro *et al.* [13]), for explicit modular generators in Kerr, so the Paley–Wiener conditions that enforce the tanh retrieval onset are preserved.

Superradiant amplification widens the onset profile but does not alter its functional form. To leading order we obtain

$$\delta(a, \Omega) \;=\; \delta_0\!\left(1 + \alpha\,\frac{a\,\Omega_H}{r_+}\right),$$

where δ_0 is the Schwarzschild onset width and α encodes the net superradiant gain. All stationary observers satisfying the timelike condition above therefore experience the same modular-retrieval law as in the static case, up to this calculable broadening.

A complete perturbative derivation, covering the full Kerr modular flow, the impact of non-commuting angular modes, and laboratory implications for rotating analogue black holes, will be explored in future work.

Author Contributions: Conceptualization, Formal analysis, Simulation design, Visualization, Writing—original draft, and Writing—review & editing, **Evlondo Cooper**. The author has read and approved the final version of the manuscript.

Funding: This research received no external funding.

Data Availability Statement: Simulation data (entropy–retrieval vectors and $g^{(2)}$ matrices), all plotting scripts, and full simulation logs are available to reviewers and qualified researchers upon request. A curated version of the Figshare record will be made publicly available upon peer-reviewed publication. An identical copy will be mirrored on GitHub.

Conflicts of Interest: The author declares no competing interests.

References

1. Akers, C.; Faulkner, T.; Lin, S.; Rath, P. The Page Curve for Reflected Entropy. *J. High Energy Phys.* **2022**, *06*, 089. https://doi.org/10.1007/JHEP06(2022)089
2. Almheiri, A.; Marolf, D.; Polchinski, J.; Sully, J. Black Holes: Complementarity or Firewalls? *J. High Energy Phys.* **2013**, 62. https://doi.org/10.1007/JHEP02(2013)062
3. Almheiri, A.; Engelhardt, N.; Marolf, D.; Maxfield, H. The Entropy of Bulk Quantum Fields and the Entanglement Wedge of an Evaporating Black Hole. *J. High Energy Phys.* **2019**, 063. https://doi.org/10.1007/JHEP12(2019)063
4. Almheiri, A.; Hartman, T.; Maldacena, J.; Shaghoulian, E.; Tajdini, A. The Entropy of Hawking Radiation. *Rev. Mod. Phys.* **2021**, *93*, 035002. https://doi.org/10.1103/RevModPhys.93.035002
5. Araki, H. Relative Entropy of States of von Neumann Algebras. *Publ. Res. Inst. Math. Sci.* **1976**, *11*, 809–833. https://www.jstage.jst.go.jp/article/kyotoms1969/11/3/11_3_809/_pdf
6. Astesiano, D.; Gautason, F. F. Supersymmetric Wormholes in String Theory. *Phys. Rev. Lett.* **2024**, *132*, 161601. https://doi.org/10.1103/PhysRevLett.132.161601

 doi:10.20944/preprints202503.2057.v3

7. Bousso, R.; Casini, H.; Fisher, Z.; Maldacena, J. Proof of a Quantum Bousso Bound. *Phys. Rev. D* **2014**, *90*, 044002. https://doi.org/10.1103/PhysRevD.90.044002
8. Bratteli, O.; Robinson, D.W. *Operator Algebras and Quantum Statistical Mechanics I: C*- and W*-Algebras, Symmetry Groups, Decomposition of States*, 2nd ed.; Springer: Berlin, Germany, 1987. https://doi.org/10.1007/978-3-662-02520-8
9. Brunetti, R.; Fredenhagen, K.; Verch, R. The Generally Covariant Locality Principle—A New Paradigm for Local Quantum Field Theory. *Commun. Math. Phys.* **2003**, *237*, 31–68. https://doi.org/10.1007/s00220-003-0815-7
10. Bueno, P.; Cano, P.A.; Hennigar, R.A. Regular Black Holes from Pure Gravity. *Phys. Lett. B* **2020**, *861*, 139260. https://doi.org/10.48550/arXiv.2403.04827
11. Casini, H.; Huerta, M.; Myers, R.C. Towards a Derivation of Holographic Entanglement Entropy. *J. High Energy Phys.* **2011**, 036. https://doi.org/10.1007/JHEP05(2011)036
12. Casini, H.; Huerta, M.; Rosabal, J. A. Remarks on Entanglement Entropy for Gauge Fields. *Phys. Rev. D* **2014**, *89*, 085012. https://doi.org/10.1103/PhysRevD.89.085012
13. Castro, A.; Maloney, A.; Strominger, A. Hidden Conformal Symmetry of the Kerr Black Hole. *Phys. Rev. D* **2010**, *82*, 024008. https://doi.org/10.1103/PhysRevD.82.024008
14. Chandrasekaran, V.; Longo, R.; Penington, G.; Witten, E. An Algebra of Observables for de Sitter Space. *J. High Energy Phys.* **2023**, 082. https://doi.org/10.1007/JHEP02(2023)082
15. Crispino, L.C.B.; Higuchi, A.; Matsas, G.E.A. The Unruh Effect and Its Applications. *Rev. Mod. Phys.* **2008**, *80*, 787–838. https://doi.org/10.1103/RevModPhys.80.787
16. D'Antoni, C.; Longo, R. Interpolation by Type I Factors and the Flip Automorphism. *J. Funct. Anal.* **2001**, *182*, 367–385. https://doi.org/10.1006/jfan.2000.3744
17. Donnelly, W.; Michel, B.; Wall, A. C. Electromagnetic Duality and Entanglement Anomalies. *Phys. Rev. D* **2017**, *96*, 045008. https://doi.org/10.1103/PhysRevD.96.045008
18. Faulkner, T.; Li, M. Asymptotically Isometric Codes for Holography. *arXiv* **2022**, arXiv:2211.12439 [hep-th]. https://doi.org/10.48550/arXiv.2211.12439
19. Hayden, P.; Preskill, J. Black Holes as Mirrors: Quantum Information in Random Subsystems. *J. High Energy Phys.* **2007**, 120. https://doi.org/10.1088/1126-6708/2007/09/120
20. Jafferis, D.L.; Lewkowycz, A.; Maldacena, J.; Suh, S.J. Relative Entropy Equals Bulk Relative Entropy. *J. High Energy Phys.* **2016**, 004. https://doi.org/10.1007/JHEP06(2016)004
21. Jafferis, D.L.; Bluvstein, D.; Himmelspach, M.; et al. Traversable Wormhole Dynamics on a Quantum Processor. *Nature* **2022**, *612*, 51–55. https://doi.org/10.1038/s41586-022-05424-3
22. Liu, H.; Vardhan, S. Entanglement Entropies of Equilibrated Pure States in Quantum Many-Body Systems and Gravity. *PRX Quantum* **2021**, *2*, 010344. https://doi.org/10.1103/PRXQuantum.2.010344
23. Longo, R. Lectures on Conformal Nets—Part I. Unpublished lecture notes, 2008. https://www.mat.uniroma2.it/~longo/Lecture-Notes_files/LN-Part1.pdf
24. Maldacena, J.; Susskind, L. Cool Horizons for Entangled Black Holes. *Fortschr. Phys.* **2013**, *61*, 781–811. https://doi.org/10.1002/prop.201300020
25. Muñoz de Nova, J. R.; Golubkov, K.; Kolobov, V. I.; Steinhauer, J. Observation of Thermal Hawking Radiation and Its Temperature in an Analogue Black Hole. *Nature* **2019**, *569*, 688–691. https://doi.org/10.1038/s41586-019-1241-0
26. Page, D.N. Average Entropy of a Subsystem. *Phys. Rev. Lett.* **1993**, *71*, 1291–1294. https://doi.org/10.1103/PhysRevLett.71.1291
27. Pastawski, F.; Yoshida, B.; Harlow, D.; Preskill, J. Holographic Quantum Error-Correcting Codes: Toy Models for the Bulk/Boundary Correspondence. *J. High Energy Phys.* **2015**, 149. https://doi.org/10.1007/JHEP06(2015)149
28. Penington, G. Entanglement Wedge Reconstruction and the Information Paradox. *J. High Energy Phys.* **2020**, *02*. https://doi.org/10.48550/arXiv.1911.11977
29. Penington, G.; Shenker, S.H.; Stanford, D.; Yang, Z. Replica Wormholes and the Black Hole Interior. *Phys. Rev. D* **2021**, *103*, 084007. https://doi.org/10.1103/PhysRevD.103.084007
30. Simpson, A. Traversable Wormholes, Regular Black Holes, and Black-Bounces. Master's Thesis, Victoria University of Wellington, New Zealand, 2021. *arXiv* **2021**, arXiv:2104.14055. https://doi.org/10.48550/arXiv.2104.14055
31. Steinhauer, J. Observation of Quantum Hawking Radiation and Its Entanglement in an Analogue Black Hole. *Nat. Phys.* **2016**, *12*, 959–965. https://doi.org/10.1038/nphys3863

 doi:10.20944/preprints202503.2057.v3

32. Srednicki, M. Chaos and Quantum Thermalization. *Phys. Rev. E* **1994**, *50*, 888–901. https://doi.org/10.1103/PhysRevE.50.888
33. Susskind, L. The World as a Hologram. *J. Math. Phys.* **1995**, *36*, 6377–6396. https://doi.org/10.1063/1.531249
34. Takesaki, M. *Theory of Operator Algebras I*; Springer: New York, NY, USA, 2002.
35. Witten, E. APS Medal for Exceptional Achievement in Research: Entanglement Properties of Quantum Field Theory. *Rev. Mod. Phys.* **2018**, *90*, 045003. https://doi.org/10.1103/RevModPhys.90.045003
36. Witten, E. Gravity and the Crossed Product. *J. High Energy Phys.* **2022**, 008. https://doi.org/10.1007/JHEP10(2022)008